SWIRL INTENSITY INFLUENCE ON INTERACTION BETWEEN NON-SWIRLING AND SWIRLING CO-AXIAL JETS IN A COMBUSTOR CONFIGURATION: LES AND MODELLING STUDY

Sanjin Šarić, Björn Kniesner, Paul Altenhöfer, Suad Jakirlić and Cam Tropea
Fachgebiet Strömungslehre und Aerodynamik, Technische Universität Darmstadt
Petersenstr. 30, D-64287 Darmstadt, Germany
saric@sla.tu-darmstadt.de, b.kniesner@sla.tu-darmstadt.de, paltenhoefer@swd-ag.de,
s.jakirlic@sla.tu-darmstadt.de, ctropea@sla.tu-darmstadt.de

Dalibor Čavar
Fluid Mechanics Section, Department of Mechanical Engineering, Technical University of Denmark
Nils Koppels Alee 403, 2800 Kgs. Lyngby, Denmark
dc@mek.dtu.dk

Branislav Basara
Advanced Simulation Technology, AVL List GmbH
Hans-List-Platz 1, A-8020 Graz, Austria
branislav.basara@avl.com

ABSTRACT

Structural characterization of flow and turbulence in the model of a tubo-annular combustion chamber is investigated computationally using LES (Large Eddy Simulation) method and the $\zeta - f$ RANS (Reynolds-averaged Navier-Stokes) model of Hanjalic et al. (2004). The latter model, representing a robust eddy-viscosity-based model of turbulence, is used in conjunction with the universal wall treatment combining the integration up to the wall and wall functions. Reference LDA (inlet section including central and annular pipes) and PIV (combustor) measurements were performed by Palm (2006). The focus of the investigation was on the swirl intensity influence on the interaction between central non-swirling stream and a swirling co-axial jet issuing from an annular inlet section in the near-field of the flue. The results obtained demonstrate gradual expansion of the free flow reversal zone into the radial direction with corner (wall-bounded) bubble being substantially suppressed. The increasing swirl intensity contributes significantly to the intensification of the radial movement associated with strong turbulence level increase in the region of the swirling shear layer, thus promoting the mixing.

INTRODUCTION

The efficiency of the entire combustion process in a gas turbine swirl combustor depends strongly on the mixing of the swirling annular jet (primary air) and the non-swirling inner jet (fuel) in its near field. A swirl-induced, recirculation zone generated in the center of a combustor enhances flame stability and is a usual design concept of combustors. Even restricting the attention only to the isothermal case, an exceedingly complex flow pattern arises. The annular swirling stream expands suddenly transforming into a curved, axisymmetric swirling shear layer within the flue. This separated shear layer bordering the separation region is highly unsteady, featured by the organized, large-scale coherent structures (characterized by both repeatable, but also non-regular unsteadiness of the oscillatory separated regions). The large majority of the computational studies of combustor configurations conducted in the past used the RANS approach. The RANS method captures well the general character of the flow but due to the statistical nature of the method, unsteady effects are only captured partially or not at all. Accordingly, the LES method becomes increasingly a tool of choice for combustor simulations. The works of Pierce and Moin (1998), Wang et al. (2004), Derksen (2005) and Garcia-Villalba and Fröhlich (2006) demonstrate a large potential of the LES method in capturing the mean flow and turbulence phenomena in these confined flows. The topic of the present study is the numerical analysis of the variable swirl intensity influence on the flow characteristics in a tubo-annular combustor chamber, which was experimentally investigated by Palm (2006). The measurements were performed over a range of swirl intensities and Reynolds numbers related to the main stream and swirling annular flow. In addition to the LES method, a novel, eddy-viscosity-based turbulence model, denoted by $\zeta - f$ (Hanjalic et al., 2004), was applied in the RANS framework. Three different cases corresponding to the swirl intensities of $S = 0.0$, 0.6 and 1.0 were simulated.

FLOW CONFIGURATION

Schematic of the flow considered is depicted in Fig. 1 with the operating flow parameters summarized in Table 1. The inner diameter of the main flow D_m is $36\,mm$, whereas the inner and outer (D_c) diameters of the annular section are $40\,mm$ and $100\,mm$, respectively. The diameter of the flue D_f is $200\,mm$. The swirl generator is based on the 'movable block' design, Leuckel (1969). By rotating an inner and an outer annular block relative to each other, varying degrees of tangential and radial channels will be created. With a pure radial inlet, a non-swirling flow is obtained, and with a pure tangential inlet, the maximum swirl is generated. To give a first impression about the flow topology in a swirl combustor, a sketch of the mean flow pattern obtained by the $\zeta - f$ model is shown in Fig. 2.

Table 1: Operating flow conditions

Parameter	Range
Reynolds number (mean flow)	$Re_m = 23500$
Mass flow rate (mean flow)	$\dot{m}_m = 0.01\, kg/s$
Reynolds number (annular flow)	$Re_c = 49530$
Mass flow rate (annular flow)	$\dot{m}_c = 0.1\, kg/s$
Swirl intensity	$S = 0.0$, 0.6 and 1.0

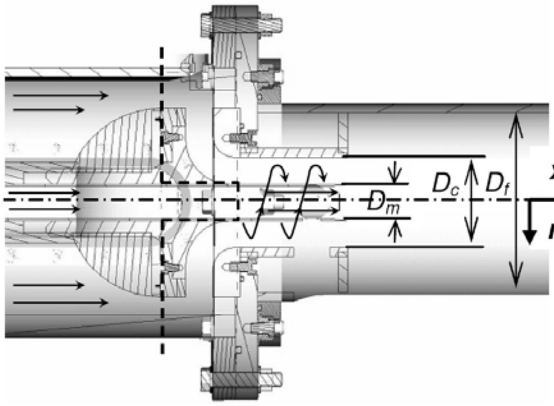

Figure 1: Schematic of the combustion chamber model

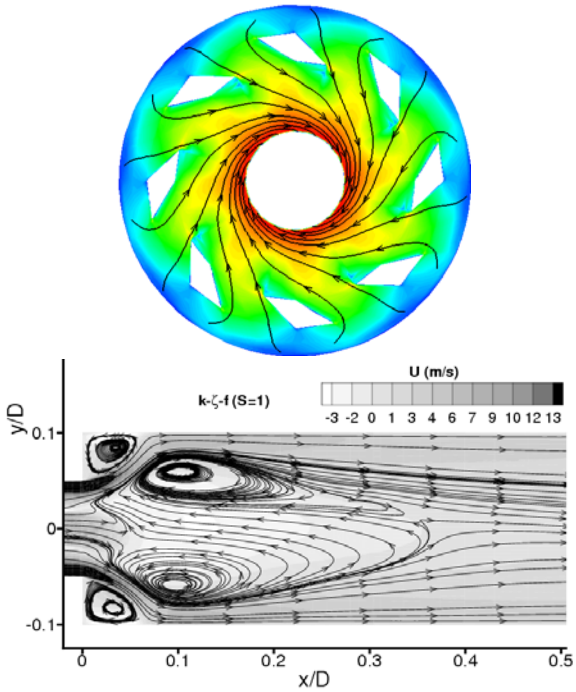

Figure 2: Mean streamline patterns within the swirl generator (upper) and the flue (lower)

COMPUTATIONAL METHOD

The RANS calculations were performed using a robust, eddy-viscosity-based $\zeta - f$ turbulence model, Hanjalic et al. (2004). This model relies on the elliptic relaxation concept providing a continuous modification of the homogeneous pressure-strain process as the wall is approached to satisfy the wall conditions, thus avoiding the need for any wall topography parameter. This model approach represents a further contribution towards more robust use of advanced closure models. The variable ζ represents the ratio v^2/k (v^2 is a scalar property in the Durbins $v^2 - f$ model, which reduces to the wall-normal stress in the near-wall region) providing more convenient formulation of the equation for ζ and especially of the wall boundary conditions for the elliptic function f. This model is used in conjunction with the so-called universal wall treatment. The latter method blends the integration up to the wall (exact boundary conditions) with the standard wall functions, enabling well-defined boundary conditions irrespective of the position of the wall-closest computational node, Popovac and Hanjalic (2007), Basara et al. (2007). This method is particularly attractive for computations of industrial flows in complex domains where higher grid flexibility, i.e. weaker sensitivity against grid non-uniformities in the near wall regions, featured by different mean flow and turbulence phenomena (flow acceleration/deceleration, streamline curvature effects, separation, etc.), is desirable. The RANS simulations were performed using the commercial CFD software package AVL SWIFT. The code employs the finite volume discretization method, which rests on the integral form of the general conservation law applied to the polyhedral control volumes. All dependent variables are stored at the geometric center of the control volume. The appropriate data structure (cell-face based connectivity) and interpolation practices for gradients and cell-face values are introduced to accommodate an arbitrary number of cell faces. The convection can be approximated by a variety of differencing schemes. The diffusion is approximated using central differencing. The overall solution procedure is iterative and is based on the SIMPLE-like segregated algorithm, which ensures coupling between the velocity and pressure fields. The computational grid used for the RANS calculations is depicted in Fig. 3. Only one fourth of the entire combustor configuration including swirl generator and inlet section (central and annular pipe), meshed by ca. 800.000 grid cells in total, was accounted for. The exception represented the case with the highest swirl intensity, which was computed accounting for the complete geometry (note a slight asymmetry in Fig. 2 lower). The solution domain includes the ring-shaped inflow plenum (Fig. 3). The length of the combustor flue corresponds to $L_x = 6D_f$. The experimental mass flow rates (Table 1) were imposed at the plenum inlet ($\dot{m}_m = 0.1\, kg/s$) and at the cross-section $x = -0.5\, m$ within the central pipe ($\dot{m}_m = 0.01\, kg/s$). The dimensionless distance of the wall-closest grid cells within the flue was in the range $1.5 - 15$ (valid for the case with $S = 0.6$).

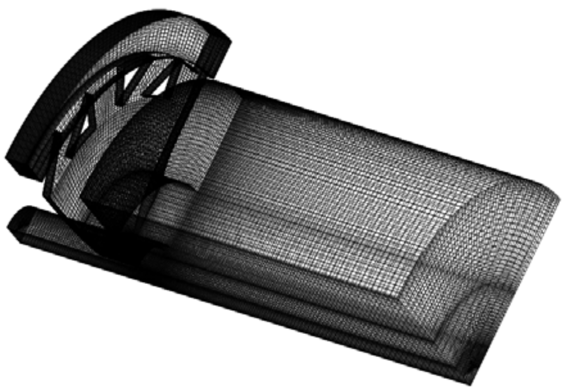

Figure 3: A detail of the numerical grid used for the RANS calculations ($S = 0.6$)

The LES simulations were performed with the in-house computer code FASTEST, based on a finite volume numerical method for solving 3-D, incompressible, filtered Navier-Stokes equations on block-structured, body-fitted, non-orthogonal meshes. A cell centered (collocated) variable arrangement and Cartesian vector and tensor components are used. The well-known SIMPLE algorithm is applied for coupling the velocity and pressure fields. The convective transport of all variables is discretized by a second-order central differencing scheme (CDS), whose stability is enhanced through the so-called deferred correction approach (the fraction of the CDS scheme in this flux blending method was 100%). Time discretization is accomplished applying the 2^{nd} order (implicit) Crank-Nicolson method. The subgrid scales are modelled with the standard Smagorinsky model ($\nu_t = (C_s\Delta)^2 \left|\overline{S}\right|$, $C_s = 0.1$). Two sets of combustor simulations were performed: one accounting for the entire inlet section including (simplified) swirl generator system (Fig. 4; the results obtained with this method are denoted by "LES" in Figs. 7- 12) and one with the swirling inflow generated computationally (not accounting for the swirl generator) at the experimental locations within the annular pipe (cross-section located $40\,mm$ upstream of the expansion; these results are denoted by "LES-f-in" in Figs. 7- 12).

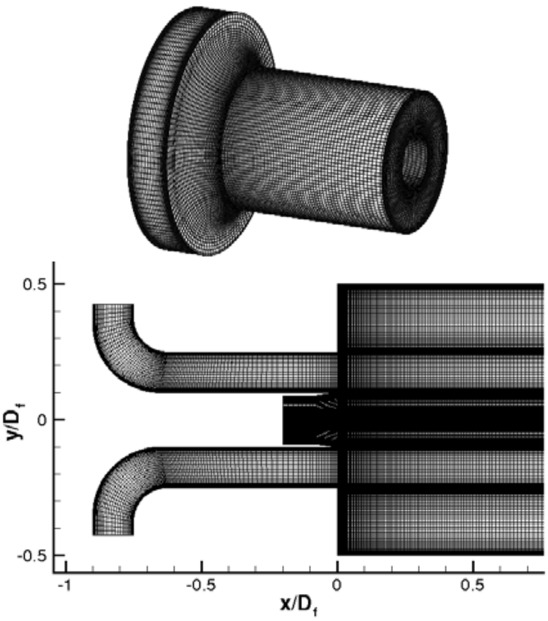

Figure 4: A simplified swirl generator (upper) including the combustor flue used for LES (lower, a grid slice in the $x-y$ plane)

In case of the latter simulations the swirling inflow was generated using the method proposed by Pierce and Moin (1998). This method assumed fully developed flow conditions, whereby the (equilibrium) swirling motion was created by introducing a fictitious pressure gradient into the momentum equation governing the circumferential velocity. The magnitude of the pressure gradient (with constant value over the cross-section) was iteratively adjusted until the computed U and W velocity fields satisfied the prescribed swirl intensity S. Additional forcing introduced into the equation governing the axial momentum had to be introduced as well (see Palm et al., 2006, for more details). The solution domain with the length of $L_x = 2.67\pi(R_c - R_m)$ was meshed by Cartesian grid with $N_x \times N_r \times N_\Theta = 64 \times 49 \times 128$ cells. The maximum value of the CFL number was 0.85. The dynamic Smagorinsky model was used for this purpose. The obtained instantaneous velocity fields across the annular pipe were prescribed for the consequent flue simulations.

The simplified swirler geometry displayed in Fig. 4 excludes the inlet plenum and the channels between movable blocks. The experimental mass flow rate was imposed at the inlet. The tangential (azimuthal) velocity component was adjusted in time until the desired swirl intensity was obtained. The solution domain consisting of the flue, simplified swirler with annular and central pipes was discretized by a Cartesian grid ($N_x \times N_r \times N_\theta$) comprising about 4.6 Mio. cells in total ($192 \times 161 \times 128$ cells in the flue, $96 \times 49 \times 128$ cells in the swirler and $19 \times 5 \times (32 \times 32)$ cells in the end part of the central pipe). The time step chosen ($\Delta t = 6 \cdot 10^{-5} s$, i.e. $7.7 \cdot 10^{-4} D_f/U_f$) corresponds to $CFL \leq 0.5$ in the largest part of solution domain. For the highest swirl intensity case ($S = 1.0$), the grid was refined in axial direction by reducing the computational domain size $L_x = 4D_f$ ($S = 0$ and 0.6) to $L_x = 2D_f$, preserving the number of computational nodes. Thus, streamwise resolution was effectively doubled. This is a compromise regarding computational effort and resolution requirements of LES. The LES computations were running two to three flow through times before taking the flow statistics which represent the average over two flow through times. Separate precursor LES of a fully developed, non-swirling (central) pipe flow corresponding to the experiment ($Re_m = 23500$) had to be conducted to generate the pipe inflow data for both sets of combustor simulations.

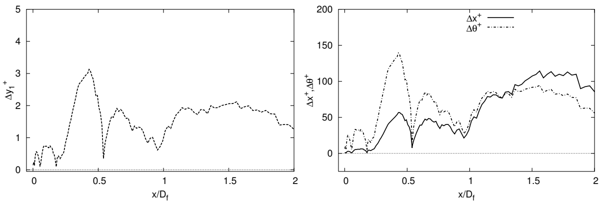

Figure 5: Wall-adjacent cell size in wall units along the wall of the combustor flue ($S = 0$)

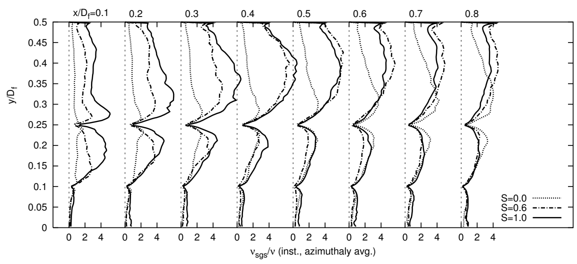

Figure 6: Profiles of the instantanoeus, azimuthaly averaged subgrid viscosity for different swirl intensities

Details about grid resolution assessment in the near-wall region of the flue can be gathered from Figs. 5 and 6. Fig. 5 shows the wall-adjacent cell size in wall units along the wall within the flue. One can see that Δy_1^+ values do not exceed three, being kept below one in the region where LES results are compared against the available experimental data. With respect to the computational cost limitations, the resolution in streamwise and azimuthal directions is also satisfactory. However, one can note that the near-wall region is not well-resolved based on the $\Delta\theta^+$ distribution. It is noted that the cell size in the θ-direction reaches its maximum at the wall, being much smaller towards the symmetry axis. Relatively coarser resolution in the near-wall region is further manifested at the subgrid viscosity profiles displayed in Fig. 6. It is clear that the core of the flue is well resolved (ν_{sgs}/ν below one), while the subgrid viscosity takes higher values in the outter region ($\nu_{sgs}/\nu \approx 6$). As it will be seen later, such a very fine grid in the core flow being extended into a slightly underesolved outer and near-wall regions, could represent one of the possible reasons for certain departures from the measured streamwise velocity profiles around the symmetry axis.

RESULTS AND DISCUSSION

Prior to considering the flow within the flue, an intensive study of the flow structure within the swirl generator system was conducted. Figs. 7 show comparison between the LDA measurements and the two sets of LES results obtained in the annular inlet section. Whereas the mean velocity profiles indicate good agreement between experiment and both LES simulations, accounting for the entire swirl generator resulted, as expected, in much better agreement with the LDA data with respect to the stress intensities.

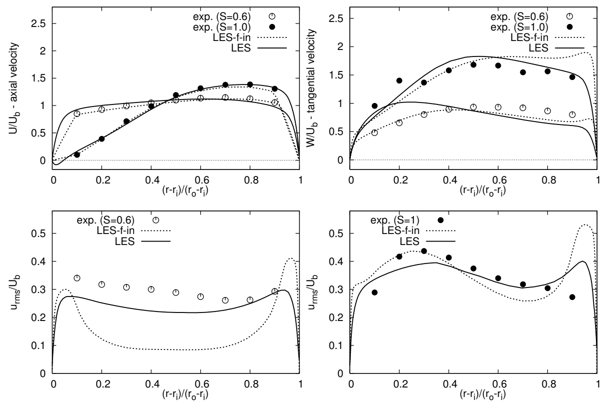

Figure 7: LES predictions of the mean velocities and streamwise turbulence intensity in the annular inlet section. U_b represents the bulk velocity within the annular pipe.

Figs. 8 to 12 show the influence of the swirl intensity on the mean flow structure illustrated by the evolution of the axial and circumferential velocity and turbulent quantity profiles at selected locations in the near field of the flow within the flue immediate after expansion featured by most intensive mixing of the swirling annular jet and non-swirling inner jet. Swirl intensity influence on the flow in terms of enhanced tendency towards the free recirculation zone generation is obvious. The ratio of the outer (annular stream at $Re_c = 49530$) flow rate $\dot{m}_c$ to the inner (mean stream at $Re_c = 23500$) one $\dot{m}_m$ was kept constant: $\dot{m}_c/\dot{m}_m = 10$. It should be noted that only the flow domain up to $x/D_f = 0.94$ and $y/D_f = 0.4$ was mapped by PIV. Also, the circumferential velocity field could not be captured by the PIV system applied. Because of that, the results of some other experimental investigations (Roback and Johnson, 1983) of a relevant tubo-annular combustor configuration at comparable flow Reynolds number ($Re_c = 47500$, $Re_m = 15900$) and swirl intenisty ($S = 0.41$) are also taken for comparison (Figs. 11-12).

The non-swirling flow configuration (Fig. 8 upper) is characterized by a long annular (wall-mounted) corner bubble. Besides a corner bubble (which is of substantially shorter length compared to the non-swirling case), the most important feature of the swirling flow configuration is a swirl-induced, free flow reversal in the core region, Figs. 8 middle and lower. A short wake region between the inner and annular streams passes into a large-eddy shear region between both recirculation zones. The most intensive turbulence production, and finally mixing, occurs just in this flow region bordering both the central and corner recirculation zones (note the peak values of the shear stress components in this region in Figs. 9). In addition to the large mean velocity gradients due to the sudden expansion, the process of turbulence generation is further influenced by an extra strain rate originating from the streamline curvature. Figs. 8

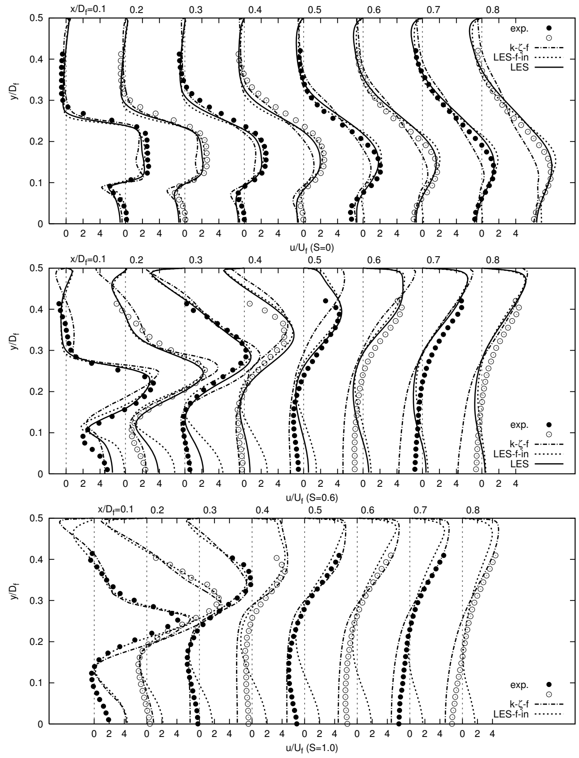

Figure 8: RANS and LES predictions of the mean streamwise velocity for various swirl intensities. U_f represents the bulk velocity within the flue.

illustrate the intensification of the velocity magnitude (with respect to both the shear layer and the back-flow region) and the strengthening of the curvature of the shear layer by increasing the swirl intensity. The radial flow becomes more intensive (see also Fig. 11), hence promoting the mixing. Whereas the annular swirling jet separates at the sharp edge of the sudden expansion, generating the corner bubble, both the separation and reattachment points of the large recirculation zone are situated in the combustor core. As expected, the highest turbulence level is captured within the shear layer regions. The Figs. 9 document also a high level of the turbulence decay at the presented combustor length.

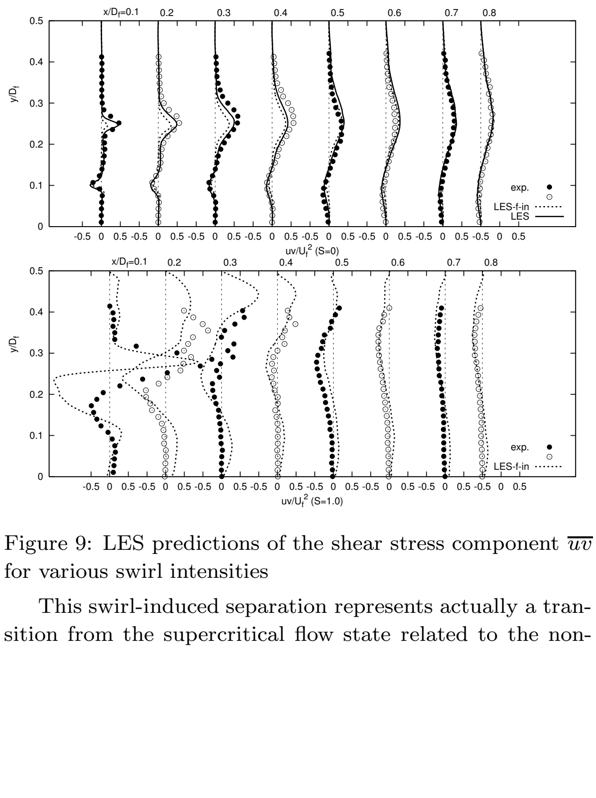

Figure 9: LES predictions of the shear stress component $\overline{uv}$ for various swirl intensities

This swirl-induced separation represents actually a transition from the supercritical flow state related to the non-swirling central stream to the sub-critical situation with respect to the flow reversal in the core (vortex breakdown phenomena; Escudier and Keller, 1985). It contributes significantly to the corner bubble shortening, Figs. 8. The increasingly curved, swirling shear layer and the position of the free separation point are of great importance for characterization of the free recirculation with respect to the mixing within the combustor. The basic mechanism behind the mixing intensification is the retardation of the axial momentum immediately after sudden expansion, manifested through its transformation into the radial and angular momentum having the highest intensity in the interface region between the corner and free bubbles. The final outcome is the propagation of the free separation point towards the flue entrance with increasing swirl intensity. In the case with moderate swirl intensity ($S = 0.6$), the separation onset, that is the free-stagnation point, is experimentally established at the position $x/D_f \approx 0.3$. The free separation point is clearly shifted upstream towards the flue entrance to the position $x/D_f \approx 0.2$ for the case with the highest swirl intensity $S = 1.0$, Figs. 8. Proper prediction of the separation onset of such a free bubble represents a special challenge for computational models. The mean velocity results displayed in Figs. 8 exhibit very good agreement with experimental data in the regions of the shear and outer layers. It is especially valid for the LES results. The $\zeta - f$ model results show, appart from some deviations within the annular jet region ($y/D_f \approx 0.1 - 0.25$) and corner bubble ($y/D_f \approx 0.3 - 0.5$) in the non-swirling and moderately swirling ($S = 0.6$) flows, generally satisfactory results. The latter statement pertains primarily to the separation onset and the free bubble size ($y/D_f(U = 0)$). However, the intensity of the reverse flow in the free recirculation zone is somewhat higher in both swirling cases (note higher negative velocity values). Both large eddy simulations result in a separation region, whose onset is not situated at the symmetry axis. The computationally obtained separation zone is lifted in the radial direction exhibiting an annular form, with a central jet going through the middle (note the continuously positive value of the centerline velocity, Fig. 8 - middle and lower). A similar outcome was obtained experimentally (Palm, 2006) but for the higher velocities of the central jet relative to the velocity of the annular jet (lower mass flow ratios, not considered in the present work). The origin of such anomaly could lay, besides the reasons pertinent to the grid resolution (see discussion corresponding to Fig. 6), in the poor representation of the swirling outflow through the boundary condition prescribed. The RANS calculations were not sensitive with respect to this issue. The conventional convective outflow was used in the LES simulations. It was not possible to mimic computationally the experimentally imposed boundary conditions. The $1.2\,m$ long flue was connected with a $6\,m$ long, flexible pipe, through which the air issued into atmosphere. The importance of the outlet boundary conditions has been recognized in some previous works. Strong influence of the combustor configuration shape (e.g., fully open, extension, contraction, etc.), i.e. of the flow structure at the outlet on the flow topology with respect to the shape and size of the core recirculation was reported by Escudier et al. (2006). The work on the computational realizations of the more adequate outlet conditions (e.g., prescription of the body force, which should replace the pressure lost in the reminder of the outlet pipe) is in progress.

Fig. 10 illustrates the evolution of the circumferential velocity field within the flue. The propagation of a strong angular momentum in the radial direction towards the combustor axis can be clearly seen. Figs. 11 (left) display the comparison of the computationally obtained results with the relevant experimental results (at somewhat lower swirl intensity: $S = 0.41$ instead of $S = 0.6$) indicating very good agreement with respect to both the profile shape and the velocity magnitude. Figs. 11 and 12 offer additional possibility for a prediction quality assessment. One can see substantial differences between two experimental data sets, related particularly to the turbulence level as well as intensity (and even the direction) of the radial motion immediately after expansion. The present predictions exhibit a higher level of agreement with the Roback and Johnsons experimental results. In the letter figures, the LES results of Pierce and Moin (1998) are also shown for the sake of comparison.

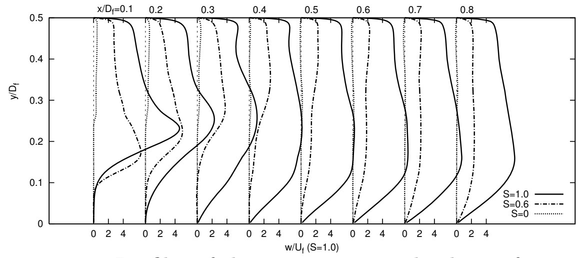

Figure 10: Profiles of the mean tangential velocity for various swirl intensities

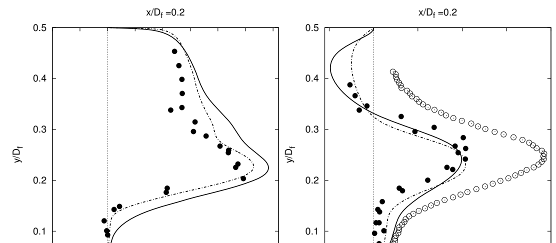

Figure 11: Comparison of the available experimenal and LES data: mean circumferential and radial velocities

Flow visualization by isosurfaces of pressure fluctuations are shown in Figs. 13 for both non-swirling ($S = 0.0$) and swirling cases ($S = 0.6$ and 1.0). With increase in the swirl intensity, the coherent structures appear to become dominant and clearly illustrate an enhanced spreding of the annular and central jets discharging into a sudden expansion, i.e. enhancement of turbulent mixing.

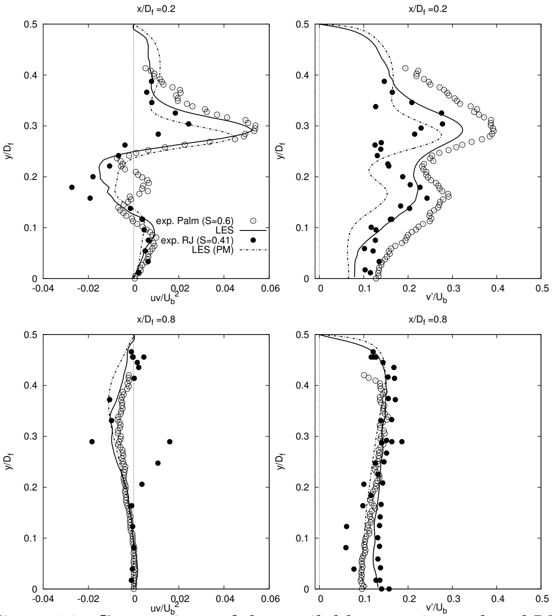

Figure 12: Comparison of the available experimenal and LES data: shear stress component and turbulence intensity

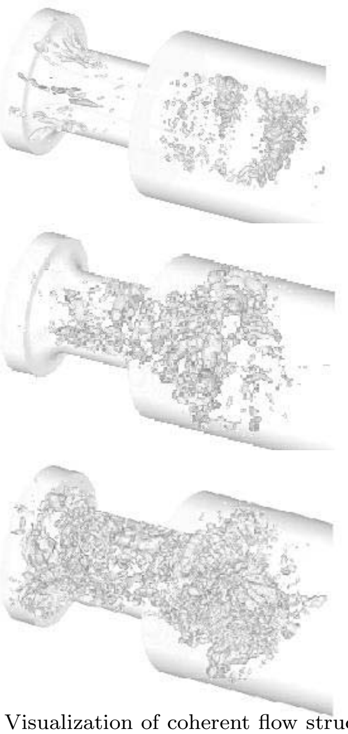
Figure 13: Visualization of coherent flow structures in LES of swirling flow in the combustor - isosurface of the instantaneous pressure fluctuation p' for various swirl intensities

CONCLUSIONS

The effects of the increasing swirl intensity on the interaction between the outer, swirling stream and the inner, non-swirling flow in the near field of a model combustor is computationally investigated applying both RANS (using the eddy-viscosity-based $\zeta - f$ model of turbulence) and LES methods. The increasingly swirled annular jet promotes an intensive mixing in the near field of combustor. It is manifested through the enhanced spreading of the flow into the radial direction and the consequent strengthening of the back-flow activity in the combustor core. The overall agreement between simulations and measurements is good. This is particularly the case in the shear layer and the outer, wall-affected flow region. Some important departures from the experimental results with respect to the mean flow structure are present in the flow core. The simulations return a ring-shaped recirculation zone with positive centerline velocities along entire flue geometry, in contrast to a closed, free separation region detected experimentally. A cause of this deviation lays most probably in the imposed outlet boundary conditions representing inadequatelly the structure of the combustor outflow. Further analysis is in progress.

Acknowledgements. The authors (S. Šarić and B. Kniesner) gratefully acknowledge financial support of the Deutsche Forschungsgemeinschaft through the grants GK "Modelling and numerical description of technical flows", the research group on "LES of complex flows" (FOR 507/1, JA 941/7-1) and the grant SFB568 "Flow and Combustion in Future Gas Turbine Combustion Chambers".

REFERENCES

AVL AST, 2004, AVL Swift/Fire Manual 8.4, AVL List GmbH, Graz

Basara, B., F. Aldudak, S. Jakirlic, K. Hanjalic, C. Tropea, M. Schrefl and J. Mayer, 2007, "Experimental Investigations and Computations of Unsteady Flows past a Real Car Using a Robust Elliptic Relaxation Closure with a Universal Wall Treatment", SAE 2007-07B-470

Derksen, J., 2005, "Simulations of confined turbulent vortex flows", *Computers and Fluids*, Vol. 34, pp. 301-318

Escudier, M.P. and Keller, J.J., 1985, "Recirculation in Swirling Flow: A Manifestation of Vortex Breakdown", *AIAA J.*, Vol. 23, No. 1, pp. 111-116

Escudier, M.P., Nickson, A.K. and Poole, R.J., 2006, "Influence of outlet geometry on strongly swirling turbulent flow through a circular pipe", *Physics of Fluids*, Vol. 18(125103)

Garcia-Villalba, M. and Fröhlich, J., 2006, "LES of a free annular swirling jet - dependence of coherent structures on a pilot jet and the level of swirl", *Int. J. Heat Fluid Flow*, Vol. 27, pp. 911-923

Hanjalic, K., Popovac, M. and Hadziabdic, M., 2004, "A robust near-wall elliptic-relaxation eddy-viscosity turbulence model for", *Int. J. Heat Fluid Flow*, Vol. 25, p. 1047-1051

Palm, R., 2006, "Experimentelle Untersuchung der Strömung und Vermischung in einem Drallbrennermodell", Ph.D. Thesis, Darmstadt University of Technology

Palm, R., Grundmann, S., Weismüller, M., Saric, S., Jakirlic, S. and Tropea, C., 2006, "Experimental characterization and modelling of inflow conditions for a gas turbine swirl combustor", *Int. J. Heat Fluid Flow*, Vol. 27, pp. 924-936

Pierce, C.D. and Moin, P., 1998, "Method for Generating Equilibrium Swirling Inflow Conditions", *AIAA J.*, Vol. 36, No. 7, pp. 1325-1327

Popovac, M. and Hanjalic, K., 2007, "Compound Wall Treatment for RANS Computation of Complex Turbulent Flows and Heat Transfer", *Flow, Turbulence and Combustion*, Vol. 78, No. 2, pp. 177-202

Roback, R. and Johnson B.V., 1983, "Mass and Momentum Turbulent Transport Experiments with Confined Swirling Coaxial Jets", NASA Contractor Report 168252

Wang, P., Bai, X.S., Wessman, M. and Klingmann, J., 2004, "LES and experimental studies of a confined turbulent swirling flow", *Physics of Fluids*, Vol. 16(9), pp. 3306-3324